Korean Journal of Geomatics
Vol. 4, No. 1 / November 2004
pp. 23~30

A Study on the Interior Orientation for Various Image Formation Sensors

Suk-Kun LEE* and Sung-Woong SHIN**

Abstract

This study aims to establish interior orientation for various types of sensors including frame cameras, panoramic cameras, line cameras, and whisk-broom scanners. To do so, this study suggests the classification of components of interior orientation of which elements are different according to the sensors. This is entailed by incorporation of sensor characteristics into mathematical models of interior orientation parameters are suggested for being used as guidelines in recovering systematic distortions. Finally, the potential errors resulted from the assumption of regarding sensor model of whisk-broom scanner model as that of push-broom scanner are discussed.

Keywords : *Interior Orientation, Frame Camera, Panoramic Linear Array Scanner, Push-broom Scanner, Whisk-broom Scanner, Distortions*

1. Introduction

Interior orientation (IO) is an important process in photogrammetry application since it plays a crucial role in obtain refined measurements of photo coordinates. The objectives of IO are to determine the camera constant and correction for systematic distortions involved in the camera system. Afore mentioned objectives are to be achieved throughout the self-calibration process. The origin of self-calibration was rooted in the development of bundle adjustment with additional parameter for aerial triangulation (Fraser, 1997). Broad accepted self-calibration process performed not only the determination of photo coordinates of principal point and focal length but the estimation of lens distortion parameters.

Even though the details of various methodologies of self-calibration are not issue in this study, it is valuable to briefly explore methods used currently. According to the usage of features (e.g point features or linear features), the self-calibration methods can be classified as point based traditional method and line based method. In the traditional method, the test field which has the numerous control points precisely surveyed is required. Nevertheless of type of imagery (either film based imagery or digital imagery), the majority of self-calibration researches including works of Heipke and others (Hepke, et al.,1992), McIntosh and others (McIntosh, 1996), and El-Habrouk and others (El-Habrouk, 1996), adopted point based method to calibrate digital camera. Using the linear feature in the self-calibration process was introduced by Brown (Brown, 1971). In his works, Brown introduced the plumb-line method that uses straight lines to derive lens distortions such as radial and decentric lens distortions. The concept of this method is that a straight line should be projected onto image space as straight line. Thus, the deviation of straightness of line in image space can be considered as effects of radial decentric lens distortions. But, this algorithm requires a separate calibration steps for determining camera constant and other systematic lens distortions (e.g. Affine deformation). Another efforts of incorporating line features in the self-calibration process can be found in works of Habib (Habib, et al., 2001). He proposed more elegant method for using linear features in self-calibration process. In this method, the linear features on object space are well represented in

*Member, Plural Prof., Yeungnam College of Science and Technology (E-mail : aimsk@hitel.net)
**Member, Ph.D. Senior Researcher, Electronics Telecommunications Research Institute (E-mail : sshin@etri.re.kr)

The manuscript for this paper was submitted for review on October 1, 2004 / accepted on October 17, 2004

image space so that the limitations of using linear feature constraints are not narrowly restricted.

Also, he overcame the drawback of separate stages IO process by proposing a test field, consisting of line and few points, where self-calibration can be performed for estimation distortion parameters and camera constants simultaneously.

Another issue of IO is automation. In conjunction with uses of image matching techmiques and computer aided environment, the interior orientation process became more robust and rapid. Schenk explained how the interior orientation process incorporates the matching algorithm and becomes autonomous process (Schenk, 2000).

However, most of aforementioned works dealt with frame camera imagery (either film based imagery or digital imagery). Thus, in this study, we analyze the mathematical models of the interior orientation of different image formation sensors. This includes the classification of various systematic distortion sources due to the imaging systems such as frame cameras, line cameras, panoramic cameras, and whisk-broom scanners. And, the factors to be known for conducting interior orientation process will be addressed explicitly.

2. Image Formaton of Sensor

2.1 Frame Camera

Frame camera system, the most fundamemtal camera system, acquires an image of area by central projection during predefined exposure time. The camera equipped lens to form an image of the scene at the focal plane. Figure1 briefly illustarates the variables involved in image formation and their geometric relationships to acquired image.

The motivation of using line cameras results from the CCD array size for recording image. In other words, using the digital frame camera induces a limitation for recording high resolution image due to the limited sizes of CCD array. This becomes more clear when we consider recording 23 cm × 23 cm aerial photo with loosely 10 ㎛ image resolution. It requires approximately 23k × 23k dimensions of CCD array which is not available currently. Now, motivation of using line cameras (e.g. panoramic linear array scanners, push-broom scanners [SPOT, IKONOS], and three line scanners [MOMS] is clear.

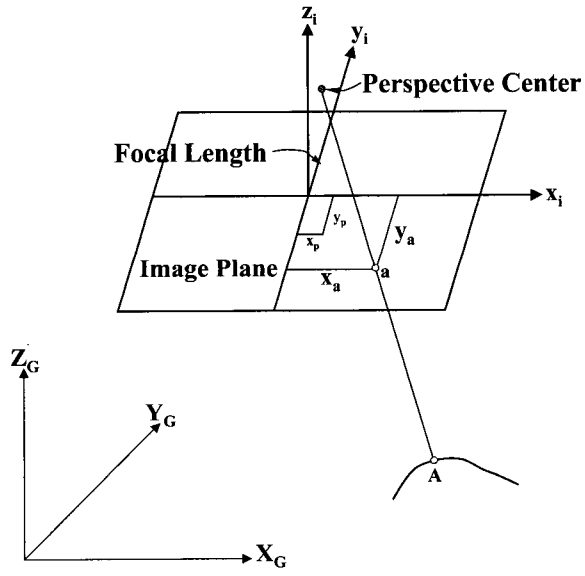

Fig. 1. Image Formation of Frame Camera.

2.2 Panoramic Linear Array Scanner

The design of panoramic camera focuses on achieving high resolution and wide swaths in one camera. The details of objects can be imaged with the narrow lens field of view (Slama et al., 1980). However, due to the lack of geometric fidelity panoramic imagery leads to several types of distortions that are not found in frame imagery (Habib et al., 1997). The Panoramic Linear Array Scanner (PLAS) is a digital imaging system, adopted principles of panoramic camera, that produces digital image as output. In this system, the sensor array is parallel to flight direction and rotates about perspective center (e.g. perpendicular to flight direction) with preset swing angle (Lee, 2002). Figure 2 conceptually illustrates the imaging system of pa-

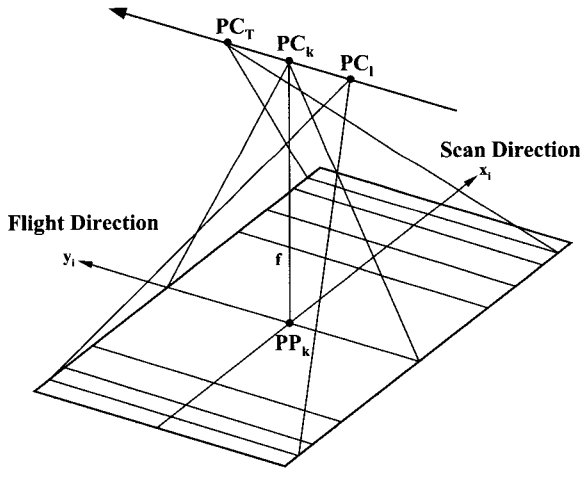

Fig. 2. Image Formation of Panoramic Linear Array Scanner.

noramic linear array scanner.

During the total scan time T [sec], the linear sensor moves along the flight direction and rotates from the first look position to the next look position. Once completing a period of scanning time of T [sec]. PLAS acquires a series of sub-swaths over the area of interest. The image coordinate system is set as follows.

- The y-axis of image coordinate coincides with the flight direction.
- The x-axis of image coordinate coincides with longitudinal direction of linear array.

2.3 Push-broom Scanner

Push-broom scanner, also called linear CCD camera or line scan device, acquires one dimensional image at a time. Unlike PLAS, push-broom scanner has linear array which is perpendicular to the flight direction. By this mechanism of movements of scanner, push-broom scanner acquires two dimensional image consisting of a combination of one dimensional image lines which have their own perspective centers. The application of this type of scanner can be found in the SPOT and IKONOS satellite imagery. Figure 3 depicts the image acquisition mechanism of push-broom scanner.

A stereo scene of push-broom scanner can be obtained when two images of the same area are acquired on different days from different orbits. This causes the time lapse between two images. In order to avoid this problem, three line scanner is introduced. The principle of imaging system of three-line scanner is the same as push-broom except it has triple linear arrays arranged for nadir looking, forward looking, and backward looking. More details about three line scanner can be found in the works of Lee (Lee, 2002).

2.4 Whisk-broom Scanner

Whisk-broom Scanner employs a single detection (rather than linear array) with a narrow fields of view swept the terrain to acquire an image (Sabins, 1997). The mechanism of imaging system of whisk-broom is basically the same as cross-track scanners. In the cross-track scanners, a faceted mirror of which rotation axis is aligned parallel th the flight direction. In other words, the mirror sweeps across the ground space with normal to the flight direction. Unlike typical cross-track scanners that have mirror sweeping to one way of direction, whisk-broom scanner has the mirror which sweeps terrains in two ways of directions (Figure 4). Landsat Thematic Mapper and AVIRIS are the typical sensors equipped with whisk-broom scanners.

Similar as PLAS, whisk-broom scanner also inherently intorduces the many sources of geometric

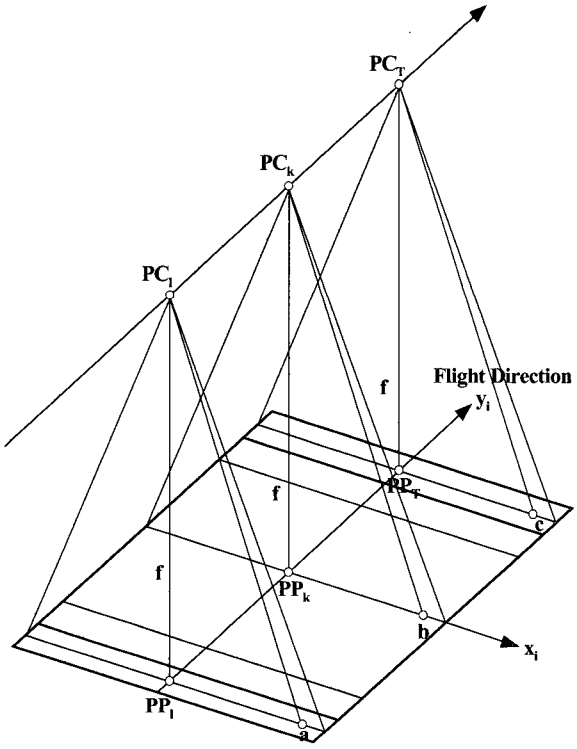

Fig. 3. Image Formation of Push-broom Scanner.

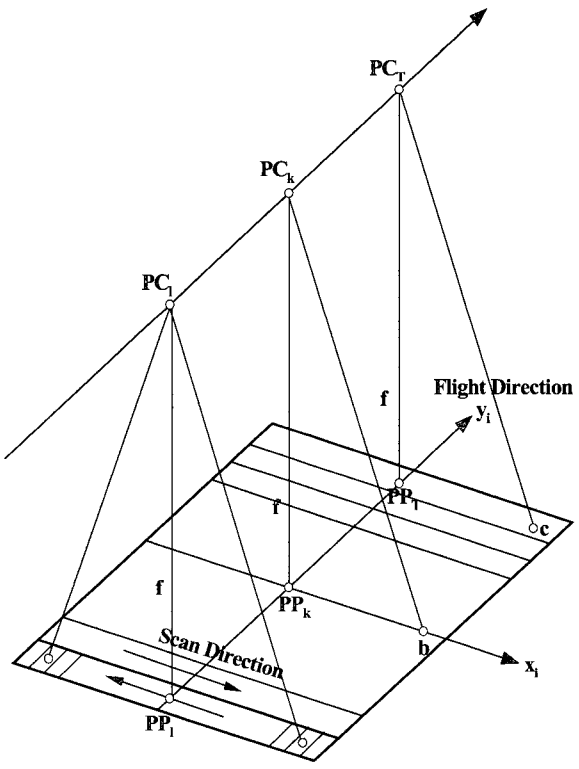

Fig. 4. Image Formation of Whisk-broom Scanner.

distortions, which can not be found in frame imagery, due to dynamic factors of imaging system. These types of distortion sources should be differentiated not only from nonsystematic distortion sources but also from static factors of imaging system.

3. Camera Calibration

The main objective of camera calibration is reconstructing the bundle of light rays, as defined by the image points and the perspective center, in such a way it is similar as possible to the incident bundle on the camera at the moment of exposure. This would entail the determinations of the following items:

- Recovering the location of the perspective center with respect to image plane
- Recovering the distortion parameters that compensate for the deviations from the assumed perspective geometry (i.e. collinearity condition).

During camera calibration, we determine the Interior Orientation Parameters (IOP) which are the principal point coordinates, the principal distance, and the image coordinate perturbations that compensate for various deviations from the collinearity model. There are four principal sources of departure from collinearity which are "physical" in nature (Fraser, 1997). These are the radial lens distortion. However, these distortion sources are only enough to depict image coordinate perturbations for imagery acquired by frame camera. Also, the image coordinate perturbations are effected by the motion of the camera systems, such as panoramic camera and whisk-broom scanner, of which exposure time is considerably longer. The relative magnitude of each one of these perturbations depends very much on the nature of the camera being employed. The net image displacement at any point is the cummulative influence of these perturbations (Habib et al., 2001). In the following sections, a variety of distortion sources are presented with examples of their effects on the image. Also, generally used math models are presented as possibly.

3.1 Distortions

① Radial lens distortions

Radial lens distortion is usually represented by polynomial series described in equation (1). The terms K_1 alone will usually suffice in medium accuracy applications. The inclusion of K_2 and K_3 terms might be required for higher accuracy and wide-angle lenses.

$$\Delta x_{RLD} = K_1(r^2-1)x + K_2(r^4-1)x + K_3(r^6-1)x$$
$$\Delta y_{RLD} = K_1(r^2-1)y + K_2(r^4-1)y + K_3(r^6-1)y \quad (1)$$

Where

$r=\sqrt{(x-x_P)^2+(y-y_P)^2}$,

x_P and y_P are the coordinates of the principal point, and K_1, K_2 and K_3 are the radial lens distortion parameters.

② Decentric lens distortions

A lack of centric of lens elements along the optical axis gives rise to the second category of lens distortion, namely, decentric distortion.

$$\Delta x_{RLD} = P_1(r^2+2x^2) + 2P_2xy$$
$$\Delta y_{RLD} = P_1(r^2+2y^2) + 2P_1xy \quad (2)$$

Where,

$r=\sqrt{(x-x_P)^2+(y-y_P)^2}$,

x_P and y_P are the coordinates of the principal point, and P_1 and P_2 are the decentric lens distortion parameters.

③ Image plane unflatness

Systematic image coordinate errors due to focal plane unflatness can limit the accuracy of photogrammetric triangulation. Radial image displacement induced by focal plane unflatness depends on the incidence angle of the imaging ray. Narrow angle lenses of long focal length are much less influenced by out-of-plane image deformation than short focal length and wide-angle lenses. To compensate for focal plane unflatness. the focal plane needs to be topographically measured. Then, a third-or fourth-order polynomial can model the resulting image coordinate perturbations.

④ In-plane distortions

In-plane distortions are usually manifested in differential scaling between x and y image coordinates. In addition, in-plane distortions introduce image axis nonorthogonality. These distortions are usually denoted Affine deformations and can be mathematically described by equation (3). One should note that Affine deformation parameters that are correlated with other IOP are eliminated(for example, shifts are eliminated since they are correlated with the principal point coordinates).

$$\Delta x_{AD} = -A_1x + A_2y$$
$$\Delta y_{AD} = A_1y \quad (3)$$

Where, A_1 and A_2 are the affine distortion parameters.

⑤ Atmospheric refraction

The light lay from the object point to the perspective center passes through different layers with different temperature, pressure and humidity. Thus, each layer has its own refractive index. Consequently, the light ray will be deviated from theoretical light ray.

$$\delta_r = \left(\frac{r^2+f^2}{f}\right)\theta \tag{4}$$

Where, δ_r is the atmospheric refraction.

⑥ Cross-track distortions

Cross-track distortion results from sampling pixels along the scan line at constant time interval. The width of a pixel is proportional to the tangent of the scan angle and wider at the both margin of the scan line. However, the data recorded and displayed at the constant rate which causes the pixels at the margins of image to be compressed relatively to those at the center. In other words, the cross-track scan angle from nadir leads to increase pixel size and spacing away from nadir. For the simplicity of understanding geometry, we assume that sensor is nadir looking (i.e. no roll angle)

$$\Delta_{CT} = f \cdot \tan(\theta_s/2) - (x_e - x_c) \tag{5}$$

Where,

Δ_{CT} is cross-track distortion at the end of scan line,

x_e is end pixel location in the scan line,

x_c is center pixel location in the scan line, and

θ_s is total scan angle for one scan line,

⑦ Scan skew distortions

The scan skew variation is caused by the forward motion of the spacecraft during the unit scan time (i.e. scan time for one scan line). This leads that the shape of ground swaths is not rectangular rather parallelogram produced distortions across the scan line.

$$\Delta_{ss_{\Delta t}} = V_c \frac{f}{H}\Delta t + \frac{L_\theta}{T}\Delta t \tag{6}$$

Where,

$\Delta_{ss_{\Delta t}}$ is scan skew at arbitrary scan time $\Delta t = 0 \sim T_\theta$,

H is altitude of sensor,

T_θ is total scan time of one scan line, and

Δt is arbitrary scan time.

⑧ Mirror velocity variations

The velocity of mirror is not constant from the start point to finish point of each scan line. This cause the mirror systematic distortions along each scan line. Thus, it is necessary to test and determine the mirror velocity variations before launch the sensor [Sabins, 1997]

⑨ Scan angle errors

The ideal scan angle is symmetric to the nadiraxis with scan angle τ. But, the real scannig system is rotated by the index error ε and the swath angle is τ^*. If swath angle can be expressed as follows:

$$\tau_i = \frac{\tau}{2} - i\frac{\tau}{n-1} \tag{7}$$

Where, τ is swath angle, i is the pulse number, and n is the total number of pulses.

Considering the index error and scan angle error, the scan angle can be rewritten as follows:

$$\tau^* = \frac{\tau+\Delta\tau}{2} - i\frac{\tau+\Delta\tau}{n-1} + \varepsilon \tag{8}$$

Where, τ_i^* is the wrong scan angel.

Then, the difference between wrong scan angle and correct one can be derived by subtract equation (7) from equation (8).

$$\Delta\tau_i^* = \tau_i^* - \tau_i = \frac{\Delta\tau}{2} - i\frac{\Delta\tau}{n-1} + \varepsilon \tag{9}$$

Now, we are about to apply equation (9) for the photogrammetric scanners such as PLAS and whisk-broom scanners. For the PLAS, linear array scanner arranged parallel to flight at i^{th} scan line, S_T be total number of scan lines, and S_i be the number of i^{th} scan line. Then, equation (9) can be modified for PLAS as follows:

$$\Delta\alpha_i^* = \alpha_i^* - \alpha_i = \frac{\Delta\alpha}{2} - S_i\frac{\Delta\alpha}{S_T - 1} + \varepsilon \tag{10}$$

Whisk-broom scanner has similar scanning system as laser scanner. The scanning direction is cross-track for each scan line. Hence, we can apply the same analogy of laser scanning system to whisk-broom scanner by denoting variables as θ_i be the scan angle at i^{th} pixel, N_T be total number of pixels, and N_i be number of i^{th} pixel. then, equation (9) can be modified for whisk-

broom as follows:

$$\Delta\theta_i^* = \theta_i^* - \theta_i = \frac{\Delta\theta}{2} - N_i\frac{\Delta\theta}{N_T - 1} + \varepsilon \quad (11)$$

3.2 Extended Collinearity Equation

Traditionally, the self-calibration parameters are determined through bundle adjustment using a large number of control points. In this study, the differences arisen when collinearity equations are modified for each sensor.

For the frame imagery, extended collinearity equations described in equations (12,13) are used and solved for:

- The ground coordinates of the points.
- The EOP of the involved imagery.
- The IOP parameters.

$$x_z = x_p - f\frac{r_{11}(X_A - X_0) + r_{12}(Y_A - Y_0) + r_{13}(Z_A - Z_0)}{r_{31}(X_A - X_0) + r_{32}(Y_A - Y_0) + r_{33}(Z_A - Z_0)} + \Delta x \quad (12)$$

$$y_a = y_p - f\frac{r_{21}(X_A - X_0) + r_{22}(Y_A - Y_0) + r_{23}(Z_A - Z_0)}{r_{31}(X_A - X_0) + r_{32}(Y_A - Y_0) + r_{33}(Z_A - Z_0)} + \Delta y \quad (13)$$

Where

$\Delta x = \Delta x_{RLD} + \Delta x_{DLD} + \Delta x_{AD} + \Delta x_{etc} + \delta_{r_x}$,

$\Delta y = \Delta y_{RLD} + \Delta y_{DLD} + \Delta y_{AD} + \Delta y_{etc} + \delta_{r_y}$

(x_a, y_a) are the observed photo coordinates of object point A,

(X_A, Y_A, Z_A) are the corresponding ground coor dinates of object point A,

(x_p, y_p) are the photo coordinates of principal point,

f is the focal length of lens,

(X_0, Y_0, Z_0) are the coordinates of the perspective center w.r.t. ground coordinate system,

$(r_{11}, \ldots, r_{33})$ are the elements of the rotation matrix R which is function of the rotation angles (ω, ϕ, κ), and

(ω, ϕ, κ) are the rotation angles w.r.t X-axis, Y-axis, Z-axis (in ground coordinate system), respectively.

For the PLAS imagery, extended collinearity equations described in equations (12,13) should be modified for considering dynamic components of imaging system.

$$x_a = x_p - f\frac{r_{11}^t(X_A - X_0^t) + r_{12}^t(Y_A - Y_0^t) + r_{13}^t(Z_A - Z_0^t)}{r_{31}^t(X_A - X_0^t) + r_{32}^t(Y_A - Y_0^t) + r_{33}^t(Z_A - Z_0^t)} \quad (14)$$

$$y_a = y_p + imc_t - f\frac{r_{21}^t(X_A - X_0^t) + r_{22}^t(Y_A - Y_0^t) + r_{23}^t(Z_A - Z_0^t)}{r_{31}^t(X_A - X_0^t) + r_{32}^t(Y_A - Y_0^t) + r_{33}^t(Z_A - Z_0^t)} \quad (15)$$

Where,

(x_a, y_a) are the photo coordinates of point a and $x_a = 0$,

imc_t is image motion compensation at time t,

(X_0^t, Y_0^t, Z_0^t) are the ground coordinates of perspective center at time t,

$(r_{11}^t, \ldots, r_{33}^t)$ are the elements of rotation matrix at time t.

Before using equations (14,15), scan angle error should be corrected through independent step of calibrating process. Then, estimated of the IOP included in equations (12,13) is performed.

For the push-broom scanners, we can expressed the extended collinearity equations as follows.

$$x_a = x_p - f\frac{r_{11}^t(X - X_0^t) + r_{21}^t(Y - Y_0^t) + r_{31}^t(Z - Z_0^t)}{r_{13}^t(X - X_0^t) + r_{23}^t(Y - Y_0^t) + r_{33}^t(Z - Z_0^t)} \quad (16)$$

$$y_a = y_p - f\frac{r_{12}^t(X - X_0^t) + r_{22}^t(Y - Y_0^t) + r_{32}^t(Z - Z_0^t)}{r_{13}^t(X - X_0^t) + r_{23}^t(Y - Y_0^t) + r_{33}^t(Z - Z_0^t)} \quad (17)$$

Where, (x_a, y_a) are the photo coordinates of point a and $y_a = 0$

Equations (16,17) also can be used for whisk-broom scanners with assumption of relatively short cross track scan time. However, it is necessary to perform the resampling, process to correct systematic error (e.g. cross-track distortions and scan skew distortions) before applying equations (16,17) for estimating IOP, Also, it is noted that another calibration process should be conducted for correction of mirror velocity variations and scan angle errors.

4. Estimate Parameters

In order to estimate IOP involved in each sensor model, we applied least squares adjustment, which minimizes the squares sum of residuals, by using Gauss-Markov model as follows:

For the full rank of matrix A, the least squares solutions can be expressed as follows:

$$y_{n\times 1} = A_{n\times m} \cdot \xi_{m\times 1} + e_{n\times 1}, \quad e \sim (0, \sigma_0^2 P^{-1}) \quad (18)$$

Where,

$y_{n\times 1}$ is observation vector (herein, photo coordinates of points),

$A_{n\times m}$ is design matrix consisting of partial derivatives of observations with respect to parameters,
$\xi_{m\times 1}$ is parameter vector to be estimated,
$\epsilon_{n\times 1}$ is random error vector,
n is the number of observations,
m is the number of parameters to be estimated,
P is the weight matrix of observations.

For the full rank of matrix A, the least square solutions can be expressed as follow:

$$\hat{\xi} = N^{-1}c, [N, c] = A^T P[A, y] \quad (19)$$

Where, $\hat{\xi}$ is estimate of parameters, $D\{\hat{\xi}\}$ is dispersion matrix of estimated parameter and $\hat{\sigma}_0^2$ is estimated variance component.

Once we estimate the IOP, we can investigate the correlations between parameters. If we find certain parameters are highly correlated to other, we can eliminate better these parameters from the adjustment model (i.e. reduce the number of parameters to be estimated). This process is important to avoid over-parameterization in adjustment process.

5. Conclusions

This study has been undertaken to establish IO models for different types of sensors.

There are various sources of systematic distortion sources due to imaging system. When classifying the distortion sources, it is necessary to differentiate between systematic distortions and nonsystematic distortions. If the effects of distortions are predictable, we can classify them as systematic distortions. Only systematic distortions are dealt in the IO procedure. The following section presents the IOP and factors to be known for establishing IO of different sensors. Table 1. summarizes that IO components to be considered for each sensor.

For the certain types of systematic distortions, it is necessary to know the variables involved in the sensor characteristics in order to recover them. Followings are the summaries of variables to be known for the correction of systematic distortions.

- Atmospheric Refraction : Focal length and EOP of sensor.
- Cross-track Distortions : Focal length, Scan angle, and Scan time.
- Scan Skew Distortions: Focal length, Altitude of sensor, Scan length (L_α for PLAS or L_θ for whisk-broom), and Scan time(T_α for PLAS or T_θ for whisk-broom).
- Scan Angle Errors: Index Error, Scan angle(or Number of scan lines for PLAS, or Number of pixels in one scan line for whisk-broom)

However, it is not necessary to estimate all IOP for sufficiently describing the specific sensor characteristics since certain IOP are highly correlated to each other. Thus, establishing sufficient IO model for specific

Table 1. IOP for different sensors.

	Sensors			
IO Components	Frame Camera	PLAS	Line camera	Whisk-broom
c	○	○	○	○
x_p, y_p	○	○	○	○
$\Delta x_{RLD}, \Delta y_{RLD}$	○	○	○	×
$\Delta x_{DLD}, \Delta y_{DLD}$	○	×	×	×
$\Delta x_{AD}, \Delta y_{AD}$	○	○	○	○
δ_r	○	○	○	○
Δ_{CT}	×	×	×	○
MVV	×	○	×	○
Δ_{ss}	×	○	×	○
$\Delta\alpha_i^*$ or $\Delta\theta_i^*$	×	○	×	○

MVV : Mirror Velocity Variations
○ : To be considered ×: Not to be considered (or negligible)

sensor require dicorrelation process that can be conducted through investigating variance-covariance matrix of estimated parameters.

Reference

1. Slama, C. C., Teurer, C. and Henriksen, S. W. (1980). Manual of Photogrammetry, 4th Ed., ASPRS, Falls Church, VA, USA.
2. Brown, D.C. (1966). Decentric distortion of lenses. Journal of Photogrammetric Engineering and Remote Sensing, 32(3):444-462.
3. Brown, D. C. (1971). Close range camera calibration. Journal of Photogrammetric Engineering and Remote Sensing, 37(8):855-866.
4. Clark, R. N., Livo, K. E. and Kovaly, R. F. (1998). Geometric Correction of AVIRIS Imagery Using On-Board Navigation and Engineering Data, Summary of 7th annual JPL Airborne Earth Science Workshop, JPL Publication 1998. Proceedings.
5. El-Habrouk, H., Li, X. P. and Faig, W. (1996). Determination of Geometric Characteristics of A Digital Camera by Self-Calibration, International Archives of Photogrammetry and Remote Sensing, Vol. XXXI, Part B1, Vienna, pp. 60-64.
6. Fraser, C. (1997). Digital self-calibration. ISPRS journal of Photogrammetry and Remote Sensing, 37(8):855-866.
7. Fraser, C. (1997). Digital camera self-calibration, ISPRS Jurnal of Photogrammetry and Remote Sensing, 52(1997): 149-159.
8. Habib, A. F., Morgan, M. and Lee, YR. (2001), Submitted to Photogrammetric Record 2001 and will Publish in October 2002.
9. Habib, A. F. (1999). GS601 Class Note, Department of Civil and Environmental Engineering and Geodetic Science, The Ohio State University. Columbus, OH, U.S.A.
10. Habib, A. F. (2000). GS725 Class Note, Department of Civil and Environmental Engineering and Geodetic Science, The Ohio State University. Columbus, OH, U.S.A.
11. Habib, A. F., Beshah, B. T. (1997). Modeling Panoramic Linear Array Scanner, Technical Report, No.443, Department of Civil and Environmental Engineering and Geodetic Science, The Ohio State University. Columbus, OH, U.S.A.
12. Heipke, C., Stephani, M., Strumz, G. and Lenz, R. (1992). Photogrammetric Calibration and Point Determination Using a Digital CCD Camera, International Archives of Photogrammetry and Remote Sensing, Vol. XXIX, Part B5, Washinton, D.C., pp. 556-560.
13. Lee, Y. (2002), Pose Estimation of Line Cameras Using Linear Features, Ph. D. Dissertation, Department of Civil and Environmental Engineering and Geodetic Science, The Ohio State University, Columbus, OH, U.S.A.
14. McIntosh, K. (1996). A Calibration Procedure for CCD Cameras, International Archives of Photogrammetry and Remote Sensing, Vol. XXXI, Part B1, Vienna, pp. 138-143.
15. Sabins, F. F. (1997). Remote Sensing: Principles and Interpretation, 3th Ed., W.H, Freeman and Company, New York, U.S.A.
16. Schaffrin, B. (1999). GS 650 Class notes, Department of Civil and Environmental Engineering and Geodetic Science, The Ohio State University. Columbus, OH, U.S.A.
17. Schenk, T. (2000). Digital Photogrammetry, Vol, I, Terra Science. Laurelville, OH, U.S.A.
18. Schenk, T. (2001). Modeling and Anayzing Systematic Errors in Airborne LaserScanner, Technical Notes in Photogrammetry, No. 19.